Trends in upper tropospheric water vapor over the Tibetan Plateau from remote sensing

Qinglong You [1,2,3]*, Zhihong Jiang[1], Yansong Bao[4], Nick Pepin[5], Klaus Fraedrich[3],

1. Climate Dynamics Research Center and Earth System Modeling Center; Key Laboratory of Meteorological Disaster, Ministry of Education; Nanjing University of Information Science and Technology (NUIST), Nanjing, 210044, China;
2. Key Laboratory of Land Surface Process and Climate Change in Cold and Arid Regions, Chinese Academy of Sciences, Lanzhou 730000, China;
3. Max Plank Institute for Meteorology, KlimaCampus, Hamburg 20144, Germany;
4. Collaborative Innovation Center on Forecast and Evaluation of Meteorological Disasters, Key Laboratory for Aerosol-Cloud-Precipitation of China Meteorological Administration, NUIST, Nanjing, 210044, China;
5. Department of Geography, University of Portsmouth, U.K.

* Corresponding author E-mail address: yqingl@126.com

Resubmitted to ***International Journal of Climatology***

Jan. 5, 2016

Abstract:

Water vapor in the upper troposphere is the dominant greenhouse gas and provides the largest feedback mechanism for amplifying climate change. However, lack of high elevation observations has limited our understating of its long term variability. In this study, the homogenized time series of the upper tropospheric water vapor (UTWV) brightness temperature (BT) over the Tibetan Plateau (TP) during 1979-2012, developed through inter-satellite calibration of high-resolution infrared radiation sounder (HIRS) channel 12 clear-sky measurements, is examined. The HIRS UTWV BT above the TP is increasing (drying), with an annual rate of 0.6 K/decade ($P<0.05$), with the largest increases above the western TP. On a seasonal basis, HIRS UTWV BT shows only slight changes during 1979-1995, but rapidly increases from 1996 to 2012. Thus, drying is concentrated during recent decades, consistent with reduced water vapor flux and relative humidity. The time series of HIRS UTWV BT is correlated with a Mongolian geopotential height index at 400 hPa and the South Asian summer monsoon derived from NCEP/NCAR reanalysis. Thus atmospheric circulation anomalies are a control of changes in UTWV. In summer, increasing horizontal divergence at 400 hPa has suppressed the upward motion of air from the lower to the upper troposphere, reducing conveyance of sensible heat to the upper troposphere and contributing to the drying observed.

Key words: Water vapor; Trend; Tibetan Plateau; UTWV

1. Introduction

Water vapor in the upper troposphere is the dominant greenhouse gas and provides a large feedback mechanism for amplifying climate change caused, for example, by anthropogenic forcings. Because it plays a major role in both radiative and hydrological feedbacks in the climate system, more attention has been paid in recent years to quantifying its spatial and temporal variability [*IPCC*, 2007; 2013; *Sherwood et al.*, 2010; *Soden*, 1998; 2000]. According to the Intergovernmental Panel on Climate Change (IPCC) Fourth Assessment Report (AR4), total column water vapor has increased over the global oceans by 1.2 ± 0.3 % per decade during 1988–2004, consistent with increases in relative humidity. This has enhanced the greenhouse effect with more water vapor stored in the atmosphere generally increasing precipitation intensity and the risk of heavy rain and snow events [*IPCC*, 2007; 2013]. This amplification highlights the importance of water vapor both as a feedback mechanism and as a potential fingerprint of anthropogenic climate change [*Soden et al.*, 2004]. In addition, water vapor acts as medium for water and heat exchange/transport in the climate system, and has linkages with the formation of clouds and precipitation [*Dai*, 2006; *Dai et al.*, 2011; *Trenberth and Guillemot*, 1998; *Trenberth et al.*, 2007]. Thus, understanding trends in high tropospheric water vapor is of great importance for understanding the global water cycle.

Many studies have investigated the accuracy of water vapor measurements comprising a multitude of datasets, including in situ observations (radiosondes), reanalyses, climate model output and remote sensing data [*Shi*, 2013; *Shi and Bates*,

2011; *Soden*, 1998; 2000; *Soden and Bretherton*, 1993; *Solomon et al.*, 2010]. Recent studies have emphasized the importance of water vapor in a climate change context. In an investigation of stratospheric processes and their role in climate (SPARC) by the world climate research program [*Kley et al.*, 2000], the authors noted that water vapor has been measured over the past 50 years using a variety of in situ and remote sensing measurement techniques which makes long-term calibration difficult.

Historically, water vapor values above the surface have been measured by sensors on radiosondes. However, these are geographically restricted, being found mostly over land in the Northern Hemisphere, and worse still, different sensors give different absolute water vapor values. Poorer instruments respond too slowly and overestimate water vapor amounts at high levels [*Shi*, 2013; *Shi and Bates*, 2011; *Shi et al.*, 2012]. *In situ* observations therefore often contains errors, biases, discontinuities and inhomogeneities, caused by the difficulties in measuring humidity, changes in hygrometers and in observing practices. Such problems have severely hampered the understanding of recent trends in water vapor [*Dai*, 2006; *Dai et al.*, 2011]. Despite these limitations, radiosondes are still widely used to provide water vapor both for field campaigns and national observing networks. These generally underestimate water vapor in the upper troposphere [*Dai*, 2006; *Dai et al.*, 2011]. Attempts to homogenize global radiosonde humidity data from the integrated global radiosonde archive (available online at www.cgd.ucar.edu/cas/catalog), found that adjusted estimates showed an increase in tropospheric water vapor on the global scale over the last few decades [*Dai et al.*, 2011].

Satellite measurements also have homogeneity problems. After intersatellite calibration, 3 decades of High-Resolution Infrared Radiation Sounder (HIRS) channel 12 clear-sky measurements were used to develop a climatologically homogenized time series of upper tropospheric water vapor (UTWV) [*Chung et al.*, 2014; *Shi*, 2013; *Shi and Bates*, 2011; *Shi et al.*, 2012], now used widely in water vapor research [*Chung et al.*, 2014; *Shi*, 2013; *Sohn et al.*, 2013]. This also showed an increase in humidity in the tropics, but decreases in the sub-tropics between 1979 and 2009. Changes in relative humidity have also been studied in model simulations [*Sherwood et al.*, 2010].

The Tibetan Plateau (TP hereafter, with the main domain of 86^{o}-106^{o}E and 26^{o}-40^{o}N) is the highest and most extensive highland in the world and has been called the "Asian water tower". In recent decades, climate change in the TP has been under increased scrutiny, not least because of the possibility of cryospheric changes amplifying the global warming signal in this region [*Kang et al.*, 2010; *You et al.*, 2008a; *You et al.*, 2010; *You et al.*, 2008b]. The distribution of atmospheric water vapor in this high elevation, semi-arid region has significant effects on climate, droughts and floods, and water balance. However, previous studies are limited due to the scarcity of ground stations and limited satellite retrievals [*Zhang et al.*, 2012; *Zhao et al.*, 2012; *Zhou et al.*, 2012]. It is also possible that the elevated surface of the TP may be a pathway for cross-tropopause transport of moisture, closely related to large-scale uplift and the descent of isentropic surfaces [*Tian et al.*, 2011]. Based on the high resolution Atmospheric Infrared Sounder (AIRS) on-board the Aqua satellite and the NASA

Water Vapor Project (NVAP), the spatial and temporal variations of tropospheric water vapor over the TP have been explored [*Zhang et al.*, 2013]. However, inter-satellite calibration has not been performed and the discussion of controlling mechanisms on water vapor changes is limited. Thus an improved understanding of tropospheric water vapor over the TP is still necessary [*Zhang et al.*, 2012; *Zhang et al.*, 2013].

This study examines annual and seasonal (winter: DJF; spring: MAM; summer: JJA; autumn: SON) characteristics of UTWV over the TP during 1979-2012 based on the inter-satellite calibration datasets of HIRS UTWV [*Shi and Bates*, 2011; *Shi et al.*, 2012]. This is accomplished using the intersatellite-based retrievals for continuous spatial and temporal coverage. The mechanisms behind UTWV trends over the TP are also explored and discussed based on atmospheric composite analysis. This study differs from previous work in that it is updated to a more recent time period (1979-2012) and is centered on the upper troposphere over the TP.

2. Data and Methods

The longest dataset of UTWV is that derived from the HIRS instrumentation satellites [*Bates and Jackson*, 2001]. A climatologically-homogenized time series of UTWV has been created through inter-satellite calibration of HIRS channel 12 clear-sky measurements [*Shi and Bates*, 2011]. Although inter-satellite biases exist which are scene temperature-dependent, an algorithm has been developed to account for such bias in brightness temperature (BT) [*Shi and Bates*, 2011; *Shi et al.*, 2008; *Shi et al.*, 2013; *Soden et al.*, 2013].

Figure 1 gives an example of the weighting functions for the HIRS channel 12 for the TP atmosphere derived from the Radiative Transfer for TOVS (RTTOV) fast radiative transfer model [*Saunders et al.*, 1999] and using National Centers for Environmental Prediction/Global Forecast System atmospheric profiles [*Kalnay et al.*, 1996]. The weighting function shows a peak around 400 hPa in the upper troposphere. Thus HIRS channel 12 is not sensitive to high terrain such as the TP. Furthermore, diurnal sampling caused by the orbital drift of the NOAA satellites has a significant effect on interpretation of HIRS radiance and retrieved products used for climate studies [*Jackson and Soden*, 2007]. Making corrections to the diurnal sampling biases is only one issue in making the HIRS data more suitable for climate studies [*Shi et al.*, 2013].

The 1979-2012 NOAA HIRS BT centered on the channel 12 water vapor absorption band was extracted for the TP region. Monthly mean BT during 1979-2012 were downloaded from ftp://eclipse.ncdc.noaa.gov/pub/Data_In_Development/hirs/hirsch12monthlygrid/, with a spatial resolution of 2.5 degrees. Positive (negative) BT anomalies represent drier (wetter) conditions in the atmosphere.

To quantify changes in large scale atmospheric circulation, monthly mean geopotential height, convergence and divergence, vertical velocity, relative humidity, and zonal and meridional wind at 400 hPa and 200 hPa were obtained from the National Centers for Environmental Prediction/National Center for Atmospheric Research (NCEP/NCAR) reanalysis [*Kalnay et al.*, 1996]. Water vapor flux was also calculated from NCEP/NCAR reanalysis data. Trends of atmospheric circulation

components were performed to represent the change in circulation in recent decades. The South Asian monsoon index is defined by the zonal wind shear between 850 hPa and 200 hPa over the domain of 40^{o}-110^{o}E and 0-20^{o}N [*Webster and Yang*, 1992]. This represents the variability of the zonal wind shear and measures the intensity of the large-scale Asian summer monsoon, and has been widely applied [*Webster and Yang*, 1992].

The Mann-Kendall test for trends and Sen's slope estimates are used to detect and quantify trends in annual and seasonal BT series [*Sen*, 1968]. A trend is considered to be statistically significant if it is statistical significance at 95% level.

3. Results

3.1 Trends in HIRS UTWV BT

Figure 2 shows the mean (left plot: K) and trend (right plot: K/decade) of HIRS UTWV BT over the TP region during 1979-2012. Differences of HIRS UTWV BT between 1996-2012 and 1979-1995 are shown in Figure 3. The time series for different regions and a summary of the magnitude of regional trends of HIRS UTWV BT are shown in Figure 4. On an annual basis, HIRS UTWV BT is lowest in the northern region, especially in Qinghai province (about 242 K) and is the highest over the southern fringe of the TP (approximately 248 K). There are also distinct seasonal patterns. HIRS UTWV BT tends to be higher in summer and lower in winter, and in between in spring and autumn, which indicates that HIRS channel 12 measurements in this region show the expected seasonal fluctuation. Similar to previous studies [*Shi*, 2013; *Shi et al.*, 2012; *Sohn et al.*, 2013], HIRS UTWV BT is shown to reflect known

spatial patterns of water vapor in the TP, capturing the mean climatology realistically.

In most regions, HIRS UTWV BT shows a positive trend during 1979-2012 (Figure 2, right panel). This trend is particularly strong in winter towards the south of the region. A comparison of HIRS UTWV BT between the first and second half of the record confirms a significant increase over nearly all of the plateau and in all seasons (Figure 3) but particularly in the south and west of the region in winter, and the north and west of the region in summer. The mean annual rate of increase over the whole record (Figure 4a) is 0.6 K/decade ($p<0.05$) with largest increases in the western TP. Again in summer increases are focused in the north-west, but in winter in the south-west. Thus although regional trend magnitudes are broadly similar in each season (ranging from 0.54K/decade in autumn to 0.65K/decade in summer), the spatial patterns are different.

Figure 4b shows that changes are focused during the second half of the record. In most seasons there are only slight changes during 1979-1995, but rapid increases during 1996-2012. This indicates that the upper troposphere over nearly all of the TP is becoming increasingly dry, but especially in the most recent two decades.

3.2 Atmospheric circulation patterns and composition

To investigate changes in circulation patterns associated with the increase in HIRS UTWV BT, the trends of atmospheric circulation (geopotential height) during 1979-2012 were examined for summer from NCEP/NCAR reanalysis [*Kalnay et al.*, 1996]. The selected region covers 0-60^{o}N and 40^{o}-140^{o}E, which includes the whole TP [*You et al.*, 2011].

An enhanced anticyclonic circulation centered on Mongolia (50°N and 105°E) (Figure 5 top plot) has developed, with the largest trends of geopotential height recorded in this region. Meanwhile, a cyclonic circulation has developed over southeastern China near 25°N and 110°E (Figure 5 bottom plot). Together this implies increased easterly flow over much of the plateau. To some extent, the change in summertime atmosphere circulation in recent decades can explain the changes of HIRS UTWV BT in the TP. Significant relationships are present between HIRS UTWV BT (Figure 6a) and a Mongolian geopotential height index (Figure 6b), defined as average 400 hPa geopotential height values over the domain of 40^{o}-55^{o}N and 90^{o}-120^{o}E from the NCEP/NCAR reanalysis [*Kalnay et al.*, 1996]. Higher values mean higher pressure and warmer air over Mongolia. The Mongolian geopotential height index has increased with more frequent positive anomalies during the second half of the record (Figure 6b). The index is positively correlated with HIRS UTWV BT over most parts of TP (Figure 7 top plot), with the regionwide correlation coefficient of 0.38 passing the 90 % significance level (Table 1). Therefore higher pressure over Mongolia in summer has been associated with upper tropospheric drying in the region, but the reasons for this relationship require further study. Previous studies show that increased geopotential height over Mongolia is consistent with rapid warming in this region, and this has decreased the summer meridional temperature gradient, which could delay and/or weaken the South Asian monsoon [*Xu and Li*, 2010; *You et al.*, 2011].

In recent decades, the South Asian summer monsoon index has weakened (Figure 6c).

Both low-level westerlies and upper-level easterlies are considerably weaker during weak monsoon years than during strong years. The South Asian summer monsoon index is negatively correlated with HIRS UTWV BT over the TP (Figure 7 bottom plot). The regionwide correlation (-0.23) suggests that advection of moisture from the southern ocean has been depressed during 1996-2012 compared with 1979-1995, also consistent with a decreasing South Asian monsoon index (Figure 6c) and a drying trend of water vapor at 400 hPa in summer over the TP.

3.3 Thermodynamic mechanism analysis

To uncover the mechanisms controlling HIRS UTWV BT a composite analysis of thermodynamic properties, including vertical velocity, velocity potential, horizontal divergence and convergence, and water vapor flux components is performed. Latitude-vertical cross-sections of vertical velocity across the TP (85^{o}-90^{o}E) in summer are shown in Figure 8a (mean conditions: 1979-2012) and 8b (trend patterns: 1979-2012). Trends of these thermodynamic properties in summer during 1979-2012 have been performed in Figure 9 and 10.

There are large negative (upward) vertical velocity anomalies between 0 and 30^{o}N from 800 hPa to 200 hPa, illustrating the dominance of upward motion in the tropics. Subsidence is focused in a narrow band around 40°N- 50°N over the northern part of the plateau (Figure 8 top plot). The trends of cross-sections of vertical velocity (Figure 8 bottom plot) display positive changes during 1979-2012, suggesting weakened uplifts of vertical velocity over the TP in summer. There is also considerable weakening around 10^{o}N. Thus over much of the plateau sensible heating

through uplift has been suppressed [*Xu and Li*, 2010]. Taken together these changes are consistent with large scale drying of the upper troposphere over the plateau. Examinations of trends of velocity potential and divergence at 400 hPa and 200 hPa show weakened western flow at 400 hPa and southeastern flow at 200 hPa (Figure 9). Increased divergence over the eastern parts of the plateau and central China in summer would encourage subsidence. Meanwhile, the drying of water vapor over the TP can be supported by reducing water vapor flux (Figure 10) and decreasing relative humidity (Figure 6d). In previous studies [*Zhu et al.*, 2011], severe and extreme droughts over the TP were related to stationary wave patterns in the upper level westerlies, linked back to eddy activities induced upstream by the North Atlantic storm track. We therefore examined the difference of zonal wind at 200 hPa in summer between 1979-1995 and 1996-2012 (not shown) to quantify changes in the strength of the upper level westerly flow. In summer, the increasing easterly flow in the north of China in the later period is clear with most of the TP exposed to increased anticyclonic circulation. The weakening in westerly winds and rapid intensification of the easterly wind at 200 hPa during summer would contribute to any drying trend observed.

4. Discussion and Conclusions

Lack of observations has limited our understating of the long-term variability of water vapor, especially in the upper troposphere. The longest dataset of UTWV is that derived from the HIRS instrumentation satellites [*Bates and Jackson*, 2001], covering a time period of 1979-2012. Satellites were designed for stratospheric monitoring and

errors increase at lower elevations [*Shi*, 2013; *Shi et al.*, 2012; *Sohn et al.*, 2013]. However, HIRS UTWV BT has been proven to minimize these difficulties and is thus widely used to determine trends of water vapor [*Shi*, 2013; *Shi et al.*, 2012; *Sohn et al.*, 2013]. HIRS UTWV BT over the TP shows a significant seasonal variation. Seasonal contrasts in the spatial distribution of water vapor are relatively small, and anomalies are controlled by the large-scale atmospheric circulation. Previous studies [*Zhang et al.*, 2012; *Zhang et al.*, 2013] also found distinct seasonal changes in water vapor.

Many atmospheric factors contribute to UTWV variation. Seasonal variations in surface temperature, convection, and monsoonal circulation, produce concomitant seasonal changes in water vapor in the troposphere but beyond this, fluctuations at shorter (synoptic) and longer (inter-annual) scales are relevant, including the quasi-biennial oscillation in the stratosphere, the El Niño-Southern Oscillation and the Tropical Intraseasonal Oscillation in the troposphere [*Shi*, 2013; *Shi and Bates*, 2011; *Shi et al.*, 2012; *Sohn et al.*, 2013]. Furthermore, UTWV in the tropics and subtropics is strongly influenced by the Hadley Cell and the Walker Circulation [*Shi and Bates*, 2011].

During 1979-2012, HIRS UTWV BT over the TP has shown a positive (drying) trend on both an annual and seasonal basis. As water vapor around 300-500 hPa has a strong influence on precipitation in the regions downstream of the TP including the valleys of the Yellow and Yangtze rivers [*Zhang et al.*, 2012; *Zhang et al.*, 2013], the drying in the upper troposphere over the TP could influence precipitation and

drought/flooding in the east of China. Meanwhile, the drying in the upper troposphere over the TP is consistent with current rapid warming and glacier shrinkage [*Kang et al.*, 2010; *Yao et al.*, 2012]. Since the 1990s, the majority of glaciers in the TP and surroundings has retreated rapidly, and glaciers in the Himalayas tend to show the greatest decreases in length and area [*Kang et al.*, 2010; *Yao et al.*, 2012]. Thus, the fast shrinking of mountain glaciers at elevations of 5000-7000 m a.s.l. since the 1990s might also be associated with the simultaneous decrease in water vapor in the upper troposphere (which encourages a negative mass balance).

UTWV at middle and higher latitudes is mostly supplied through transport from the tropics through mesoscale convection, or by extratropical cyclones. Dry air can be transported from the subtropics or from the extratropical lower stratosphere [*Kley et al.*, 2000]. Thus, the drying in the upper troposphere over the TP must also relate to changes in atmospheric transport. In summer, enhanced anticyclonic circulation centered on Mongolia and cyclonic circulation in the southeast of China both support a long-term change in atmospheric transport. This along with a weakening South Asian summer monsoon has accounted for some of the drying observed. A schematic diagram which illustrates the factors supporting the drying trend evident in HIRS UTWV BT over the TP is summarized in Figure 11. Clearly further investigation of the mechanisms therein is required by both analysis of observations and through climate modeling.

Acknowledgments. This study is supported by the State Key Program of National Natural Science Foundation of China (41230528), National Natural Science Foundation of China (91437216), Jiangsu Specially-Appointed Professor project and Jiangsu Natural Science Funds for Distinguished Young Scholar "BK20140047". This study is also funded by Opening Research Foundation of Key Laboratory of Land Surface Process and Climate Change in Cold and Arid Regions, Chinese Academy of Sciences (LPCC201512) and "the Priority Academic Program Development of Jiangsu Higher Education Institutions" (PAPD). The ESMC Contribution Number is No.84. Observations are provided by the National Meteorological Information Center, China Meteorological Administration (NMIC/CMA) (http://cdc.cma.gov.cn/home.do), and NCEP/NCAR reanalysis is provided by NOAA/OAR/ESRL PSD, Boulder, Colorado, USA, from their website at http://www.cdc.noaa.gov/. The NOAA HIRS BT centered on the channel 12 water vapor data is from ftp://eclipse.ncdc.noaa.gov/pub/Data_In_Development/hirs/hirsch12monthlygrid/. We are very grateful to the reviewers for their constructive comments and thoughtful suggestions.

References

Bates, J. J., and D. L. Jackson (2001), Trends in upper-tropospheric humidity, *Geophysical Research Letters*, *28*(9), 1695-1698, doi:10.1029/2000gl012544.

Chung, E.-S., B. Soden, B. Sohn, and L. Shi (2014), Upper-tropospheric moistening in response to anthropogenic warming, *Proceedings of the National Academy of Sciences*, *111*(32), 11636-11641.

Dai, A. (2006), Recent climatology, variability, and trends in global surface humidity, *Journal of Climate*, *19*(15), 3589-3606, doi:10.1175/jcli3816.1.

Dai, A., J. Wang, P. W. Thorne, D. E. Parker, L. Haimberger, and X. L. Wang (2011), A New Approach to Homogenize Daily Radiosonde Humidity Data, *Journal of Climate*, *24*(4), 965-991, doi:10.1175/2010jcli3816.1.

IPCC (2007), Summary for Policymakers of Climate change 2007: The Physical Science Basis. Contribution of Working Group I to the Fourth Assessment Report of the Intergovernmental Panel on Climate Change *Cambridge, UK: Cambridge University Press*.

IPCC (2013), Summary for Policymakers of Climate change 2013: The Physical Science Basis. Contribution of Working Group I to the Fifth Assessment Report of the Intergovernmental Panel on Climate Change *Cambridge, UK: Cambridge University Press*.

Jackson, D. L., and B. J. Soden (2007), Detection and correction of diurnal sampling bias in HIRS/2 brightness temperatures, *Journal of Atmospheric and Oceanic Technology*, *24*(8), 1425-1438.

Kalnay, E., et al. (1996), The NCEP/NCAR 40-year reanalysis project, *Bulletin of the American Meteorological Society*, *77*(3), 437-471.

Kang, S. C., Y. W. Xu, Q. L. You, W. A. Flugel, N. Pepin, and T. D. Yao (2010), Review of climate and cryospheric change in the Tibetan Plateau, *Environmental Research Letters*, *5*(1), 015101, doi:10.1088/1748-9326/5/1/015101.

Kley, D., J. M. Russell III, and C. Phillips (2000), SPARC Assessment of upper tropospheric and stratospheric water vapour, *World Climate Research Programme, Geneva*, WMO/TD-143.

Saunders, R., M. Matricardi, and P. Brunel (1999), An improved fast radiative transfer model for

assimilation of satellite radiance observations, *Q. J. R. Meteorol. Soc.*, *125*(556), 1407-1425.

Sen, P. K. (1968), Estimates of regression coefficient based on Kendall's tau, *Journal of the American Statistical Association*, *63*, 1379-1389.

Sherwood, S. C., W. Ingram, Y. Tsushima, M. Satoh, and M. Roberts (2010), Relative humidity changes in a warmer climate, *Journal of Geophysical Research-Atmospheres*, *115*, D09104.

Shi, L. (2013), Intersatellite Differences of HIRS Longwave Channels Between NOAA-14 and NOAA-15 and Between NOAA-17 and METOP-A, *IEEE Transactions on Geoscience and Remote Sensing*, *51*(3), 1414-1424, doi:10.1109/tgrs.2012.2216886.

Shi, L., and J. J. Bates (2011), Three decades of intersatellite-calibrated High-Resolution Infrared Radiation Sounder upper tropospheric water vapor, *Journal of Geophysical Research-Atmospheres*, *116*, D04108, doi:D0410810.1029/2010jd014847.

Shi, L., J. J. Bates, and C. Y. Cao (2008), Scene Radiance-Dependent Intersatellite Biases of HIRS Longwave Channels, *Journal of Atmospheric and Oceanic Technology*, *25*(12), 2219-2229, doi:10.1175/2008jtecha1058.1.

Shi, L., G. Peng, and J. J. Bates (2012), Surface Air Temperature and Humidity from Intersatellite-Calibrated HIRS Measurements in High Latitudes, *Journal of Atmospheric and Oceanic Technology*, *29*(1), 3-13, doi:10.1175/jtech-d-11-00024.1.

Shi, L., C. Schreck III, and V. John (2013), HIRS channel 12 brightness temperature dataset and its correlations with major climate indices, *Atmospheric Chemistry and Physics*, *13*(14), 6907-6920.

Soden, B. J. (1998), Tracking upper tropospheric water vapor radiances: A satellite perspective, *Journal of Geophysical Research-Atmospheres*, *103*(D14), 17069-17081, doi:10.1029/98jd01151.

Soden, B. J. (2000), Enlightening water vapour, *Nature*, *406*(6793), 247-248, doi:10.1038/35018666.

Soden, B. J., and F. P. Bretherton (1993), Upper tropospheric relative humidity from teh GOES 6.7um channel: Method and climatology for July 1987, *Journal of Geophysical Research-Atmospheres*, *98*(D9), 16669-16688, doi:10.1029/93jd01283.

Soden, B. J., D. D. Turner, B. M. Lesht, and L. M. Miloshevich (2004), An analysis of satellite, radiosonde, and lidar observations of upper tropospheric water vapor from the Atmospheric Radiation Measurement Program, *Journal of Geophysical Research-Atmospheres*, *109*(D4), D04105, doi:10.1029/2003jd003828.

Soden, B. J., S.-W. Yeh, J. Schmetz, and H.-J. Song (2013), Observational evidences of Walker circulation change over the last 30 years contrasting with GCM results, *Climate Dynamics*, *40*(7-8), 1721-1732.

Sohn, B. J., S. W. Ye, S. J., and H. J. Song (2013), Observational evidences of Walker circulation change over the last 30 years contrasting with GCM results, *Climate Dynamics*, *40*, 1721-1732.

Solomon, S., K. H. Rosenlof, R. W. Portmann, J. S. Daniel, S. M. Davis, T. J. Sanford, and G.-K. Plattner (2010), Contributions of Stratospheric Water Vapor to Decadal Changes in the Rate of Global Warming, *Science*, *327*(5970), 1219-1223, doi:10.1126/science.1182488.

Tian, W., H. Tian, S. Dhomse, and W. Feng (2011), A study of upper troposphere and lower stratosphere water vapor above the Tibetan Plateau using AIRS and MLS data, *Atmospheric Science Letters*, *12*(2), 233-239, doi:10.1002/asl.319.

Trenberth, K. E., and C. J. Guillemot (1998), Evaluation of the atmospheric moisture and hydrological cycle in the NCEP/NCAR reanalyses, *Climate Dynamics*, *14*(3), 213-231,

doi:10.1007/s003820050219.

Trenberth, K. E., L. Smith, T. Qian, A. Dai, and J. Fasullo (2007), Estimates of the global water budget and its annual cycle using observational and model data, *Journal of Hydrometeorology*, *8*(4), 758-769, doi:10.1175/jhm600.1.

Webster, P. J., and S. Yang (1992), Monsoon and ENSO: Selectively interactive systems, *Q. J. R. Meteorol. Soc.*, *118*(507), 877-926.

Xu, L., and Y. Q. Li (2010), Reexamining the impact of Tibetan snow anomalies to the East Asian summer monsoon using MODIS snow retrieval, *Climate Dynamics*, *35*(6), 1039-1053, doi:10.1007/s00382-009-0713-6.

Yao, T. D., et al. (2012), Different glacier status with atmospheric circulations in Tibetan Plateau and surroundings, *Nature climate change*, *2*(9), 663-667, doi:10.1038/nclimate1580.

You, Q. L., S. C. Kang, E. Aguilar, N. Pepin, W. A. Flugel, and Y. P. Yan (2011), Changes in daily climate extremes in China and their connection to the large scale atmospheric circulation during 1961-2003, *Climate Dynamics*, *36*, 2399-2417.

You, Q. L., S. C. Kang, E. Aguilar, and Y. P. Yan (2008a), Changes in daily climate extremes in the eastern and central Tibetan Plateau during 1961-2005, *Journal of Geophysical Research-Atmospheres*, *113*, D07101, doi:10.1029/2007jd009389.

You, Q. L., S. C. Kang, N. Pepin, W. A. Flugel, Y. P. Yan, H. Behrawan, and J. Huang (2010), Relationship between temperature trend magnitude, elevation and mean temperature in the Tibetan Plateau from homogenized surface stations and reanalysis data, *Global and Planetary Change*, *71*(1-2), 124-133, doi:10.1016/j.gloplacha.2010.01.020.

You, Q. L., S. C. Kang, N. Pepin, and Y. P. Yan (2008b), Relationship between trends in

temperature extremes and elevation in the eastern and central Tibetan Plateau, 1961-2005, *Geophysical Research Letters*, *35*, L04704.

Zhang, Y., D. Wang, P. Zhai, and G. Gu (2012), Applicability of AIRS Monthly Mean Atmospheric Water Vapor Profiles over the Tibetan Plateau Region, *Journal of Atmospheric and Oceanic Technology*, *29*(11), 1617-1628, doi:10.1175/JTECH-D-11-00207.1.

Zhang, Y., D. Wang, P. Zhai, G. Gu, and J. He (2013), Spatial Distributions and Seasonal Variations of Tropospheric Water Vapor Content over the Tibetan Plateau, *Journal of Climate*, *26*(15), 5637-5654, doi:10.1175/JCLI-D-12-00574.1.

Zhao, T., A. Dai, and J. Wang (2012), Trends in Tropospheric Humidity from 1970 to 2008 over China from a Homogenized Radiosonde Dataset, *J. Clim.*, *25*(13), 4549-4567, doi:10.1175/jcli-d-11-00557.1.

Zhou, S., P. Wu, C. Wang, and J. Han (2012), Spatial distribution of atmospheric water vapor and its relationship with precipitation in summer over the Tibetan Plateau, *J. Geogr. Sci.*, *22*(5), 795-809, doi:10.1007/s11442-012-0964-8.

Zhu, X. H., O. Bothe, and K. Fraedrich (2011), Summer atmospheric bridging between Europe and East Asia: Influences on drought and wetness on the Tibetan Plateau *Quaternary International*, *236*, 151-157.

Table 1. Correlation coefficients between high-resolution infrared radiation sounder (HIRS) upper tropospheric water vapor (UTWV) brightness temperature (BT) and Mongolian geopotential height index at 400 hPa, South Asian monsoon index and relative humidity at 400 hPa in summer during 1979-2012

	Mongolian geopotential height index at 400 hPa	South Asian monsoon index	Relative humidity at 400 hPa
HIRS UTWV BT			
	0.38*	-0.23	-0.65**

Correlation marked ** is significant at the 0.1 level; Correlation marked * is significant at the 0.05 level;

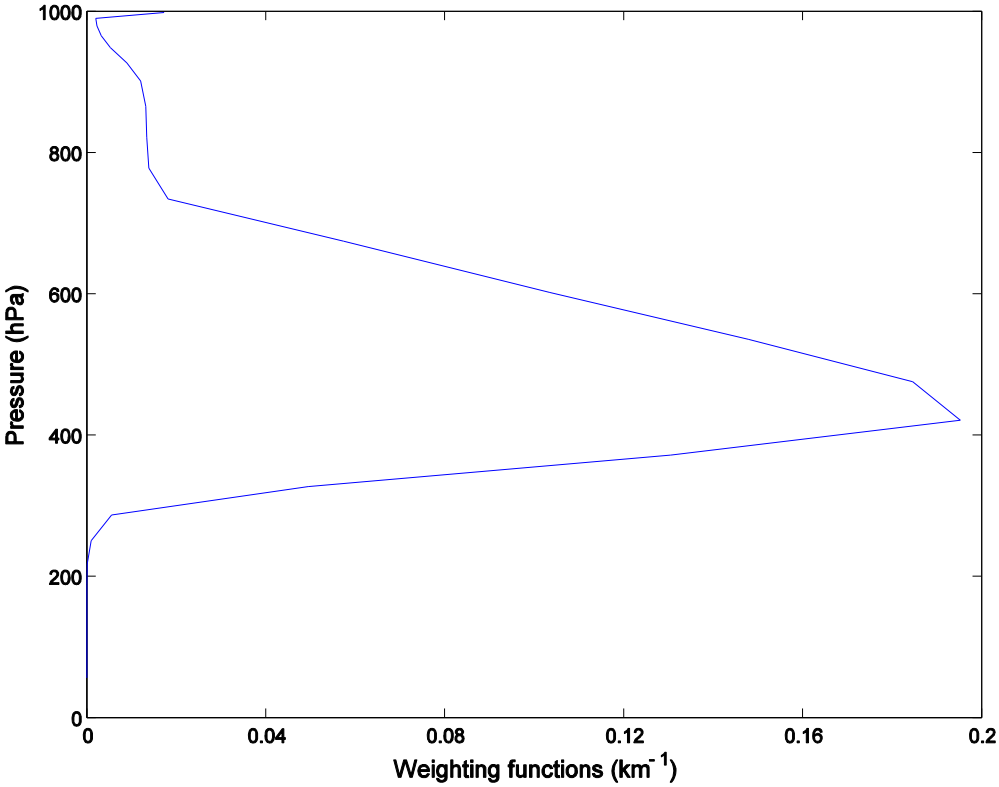

Figure 1. HIRS channel 12 weighting function.

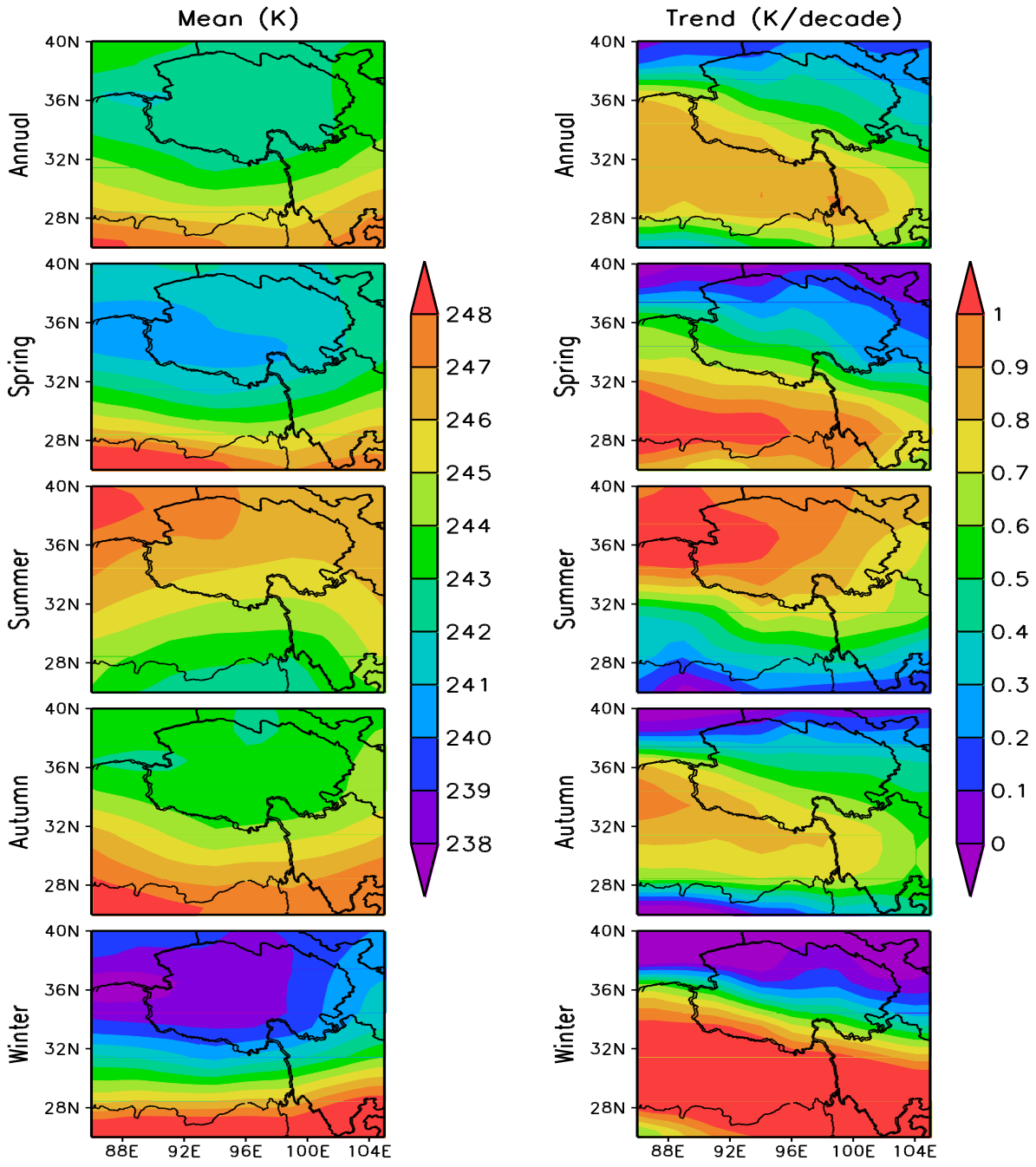

Figure 2. Mean (left plot) and trend (right plot) of HIRS UTWV BT over the Tibetan Plateau on an annual and seasonal basis during 1979-2012. The units of mean and trend of HIRS UTWV BT are Kelvin and Kelvin/decade, respectively. The trend is calculated by the Mann-Kendall statistical test.

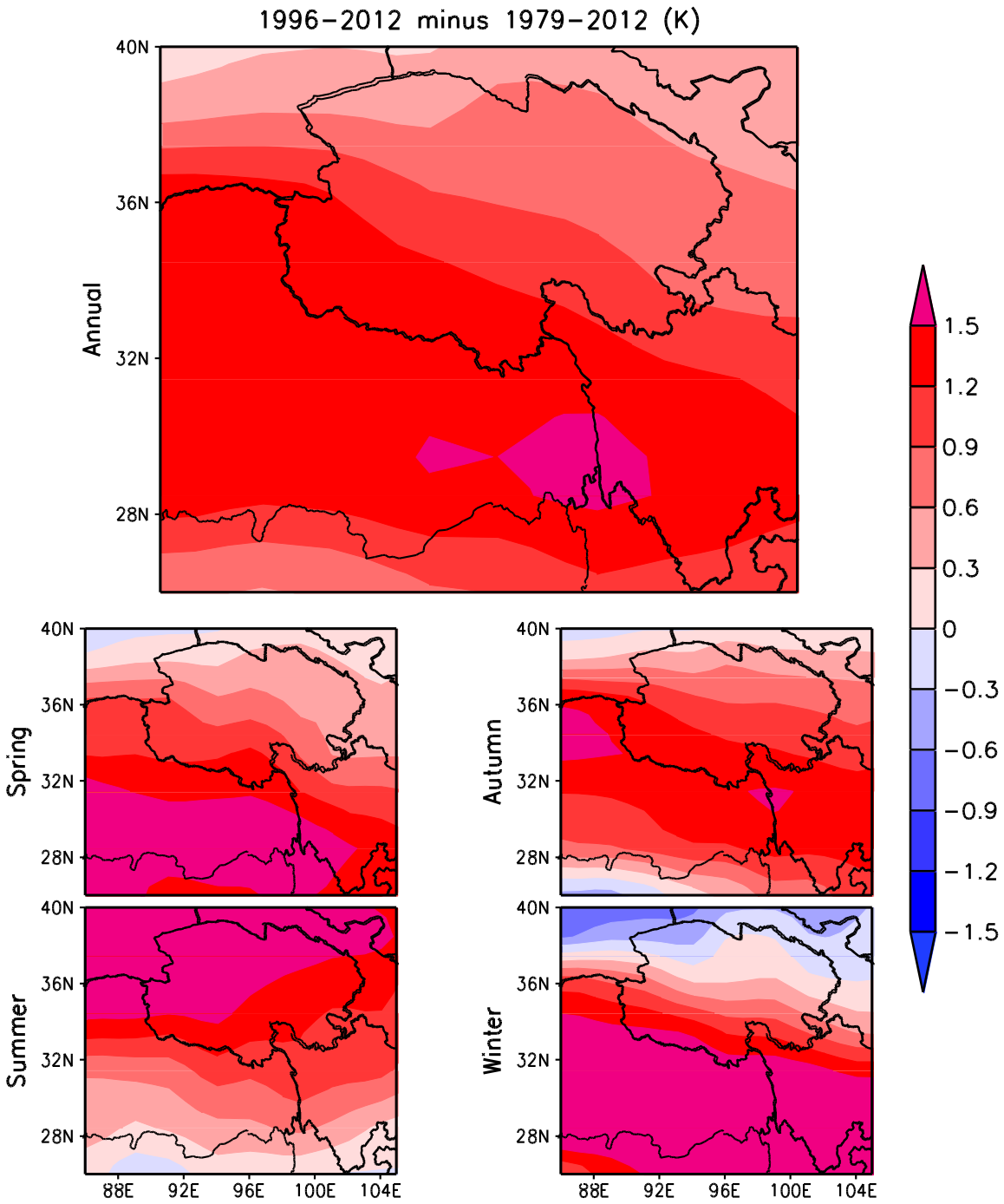

Figure 3. Differences in HIRS UTWV BT (K) over the Tibetan Plateau on an annual and seasonal basis between 1996-2012 and 1979-1995.

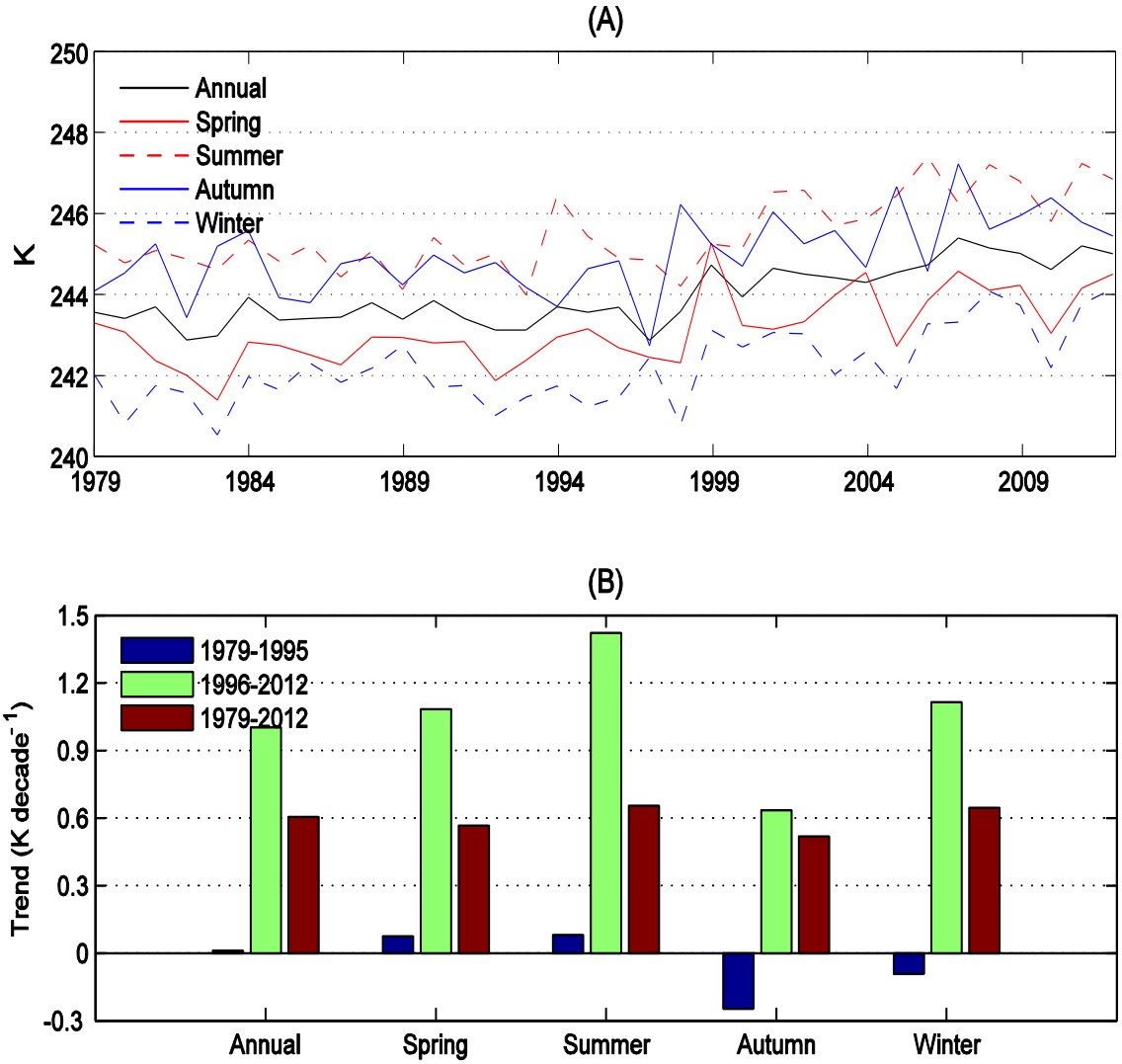

Figure 4. Time series (A) of HIRS UTWV BT over the Tibetan Plateau on an annual and seasonal basis during 1979-2012. Regional trend magnitudes (B) are summarized during 1979-2005, 1996-2012 and 1979-2012, respectively.

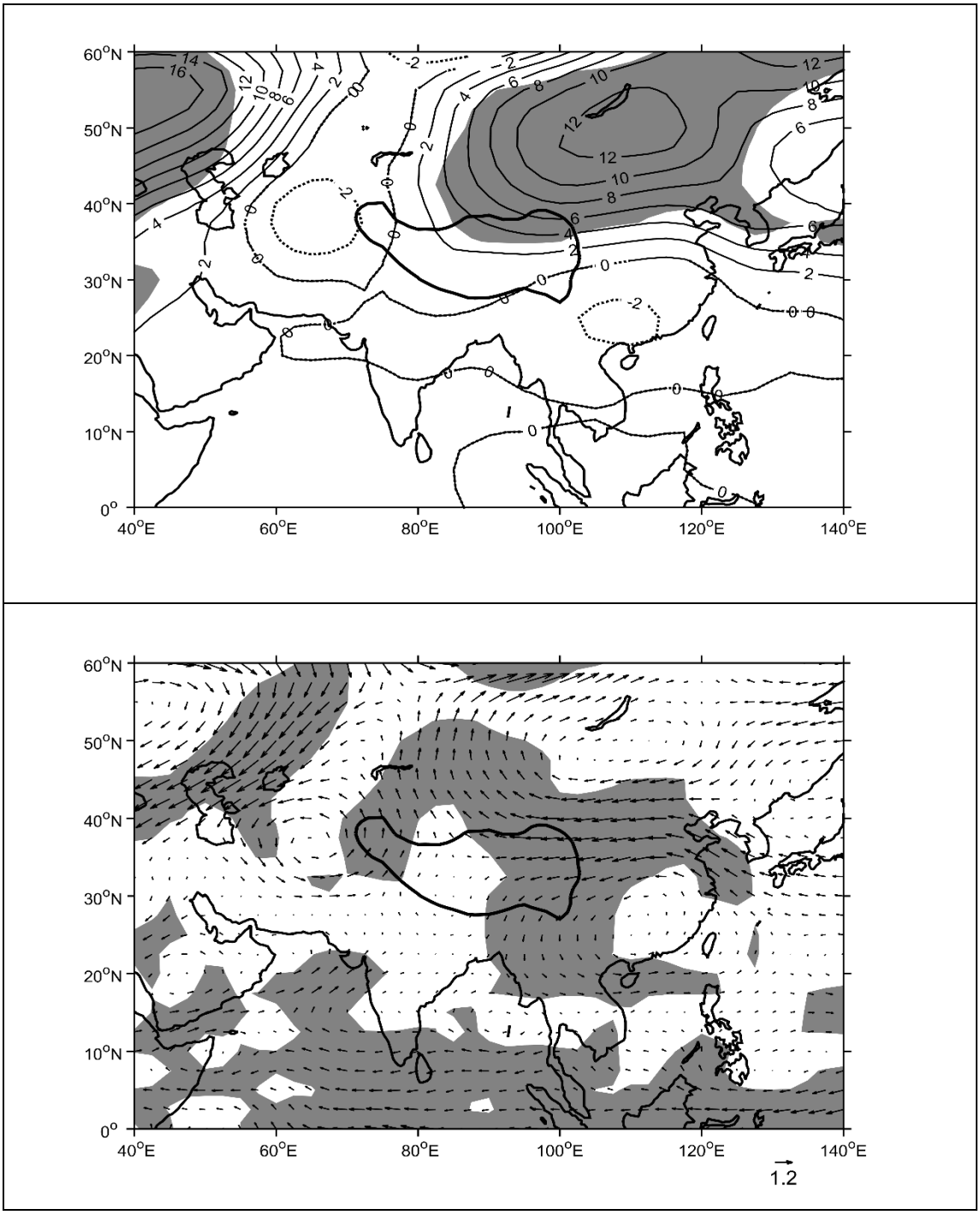

Figure 5. Trends of geopotential height (top plot, unit: geopotential height meter (ghm)/decade) and wind speed (bottom plot, unit: m/s/decade) at 400 hPa in summer during 1979-2012.

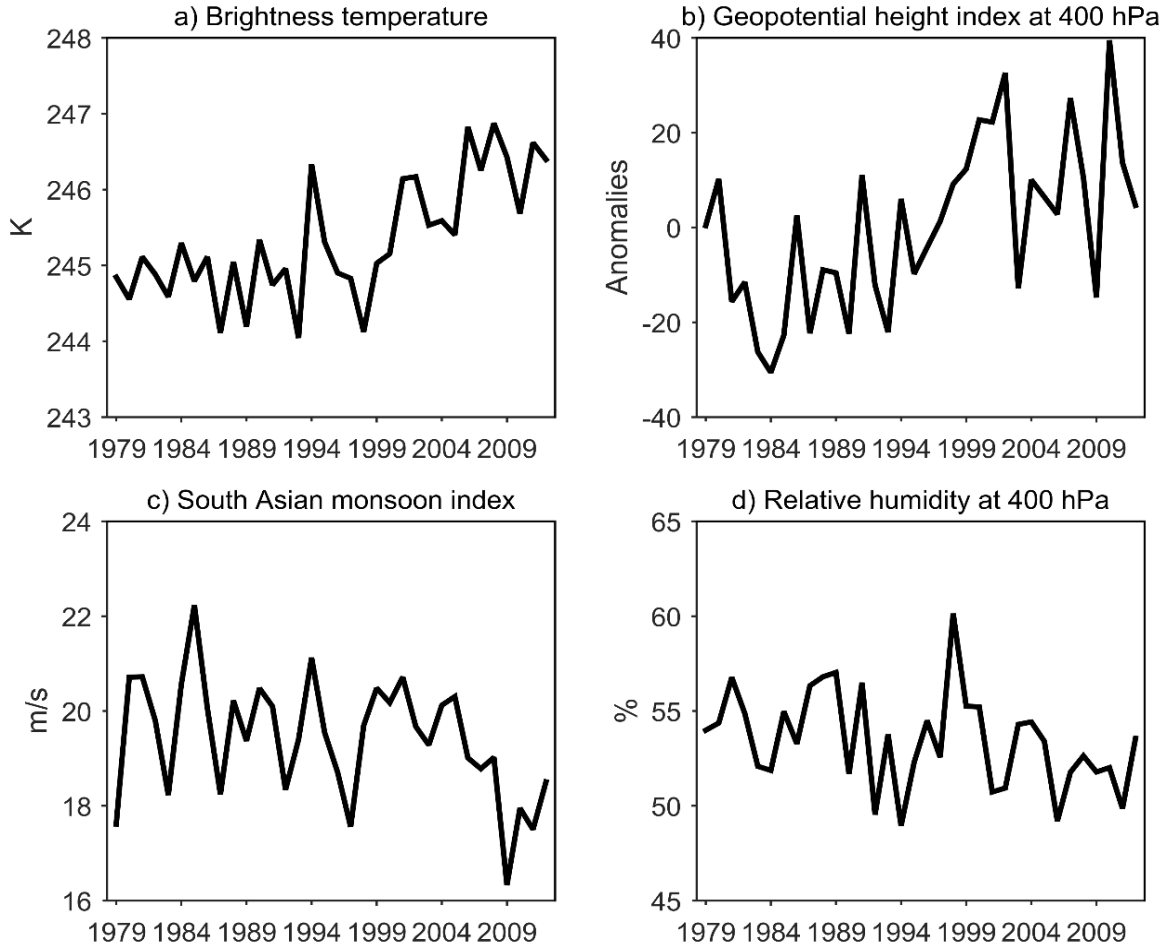

Figure 6. Time series of a) the HIRS UTWV BT over the Tibetan Plateau, b) Mongolian geopotential height index at 400 hPa, c) South Asian monsoon index, and d) relative humidity in the Tibetan Plateau at 400 hPa in summer during 1979-2012.

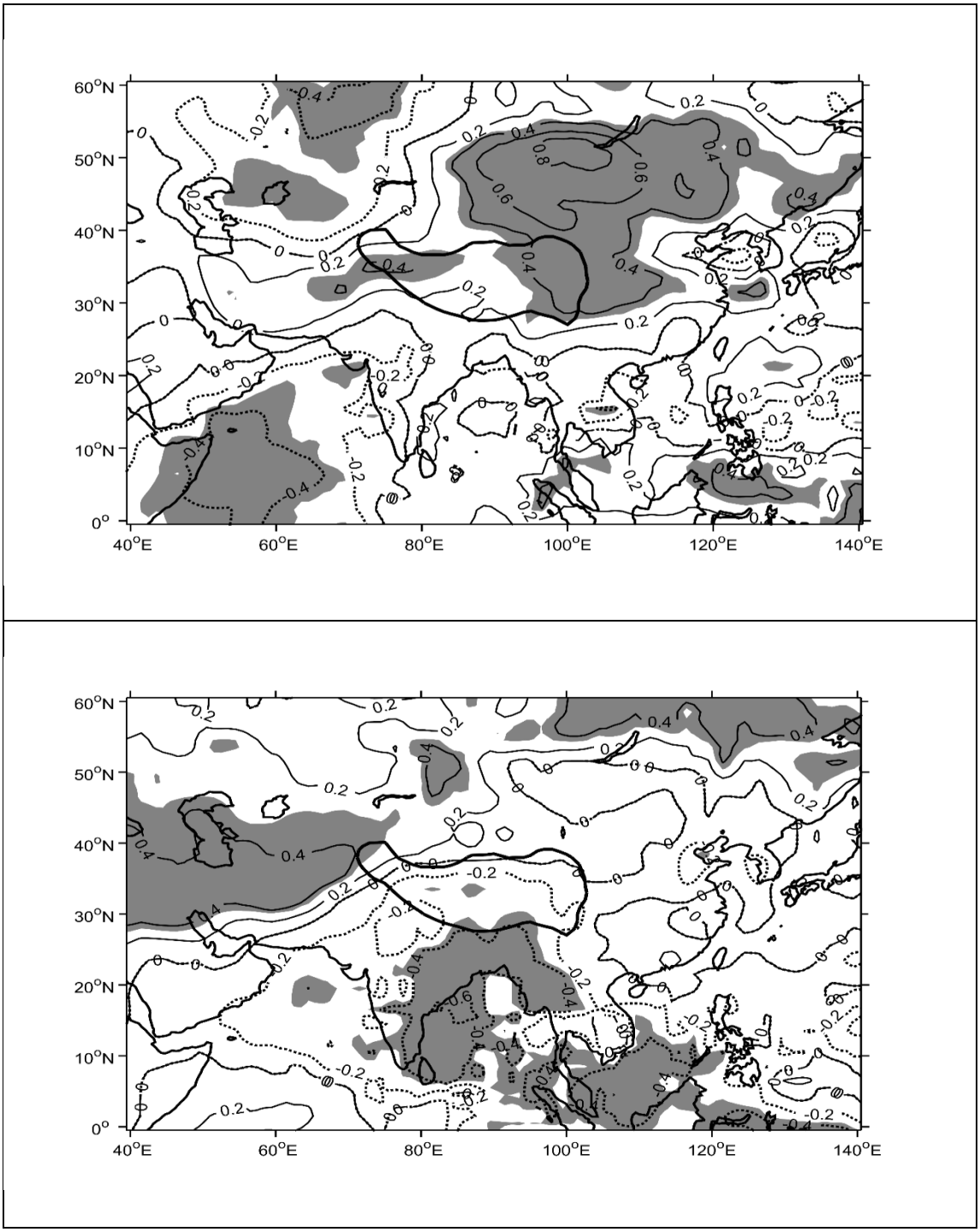

Figure 7. The spatial patterns of correlation coefficients between HIRS UTWV BT over the Tibetan Plateau and Mongolian geopotential height index (top plot), South Asian monsoon index (bottom plot) in summer during 1979-2012. Correlation coefficients significant at $p<0.05$ are shaded. The blue line represents the TP boundary.

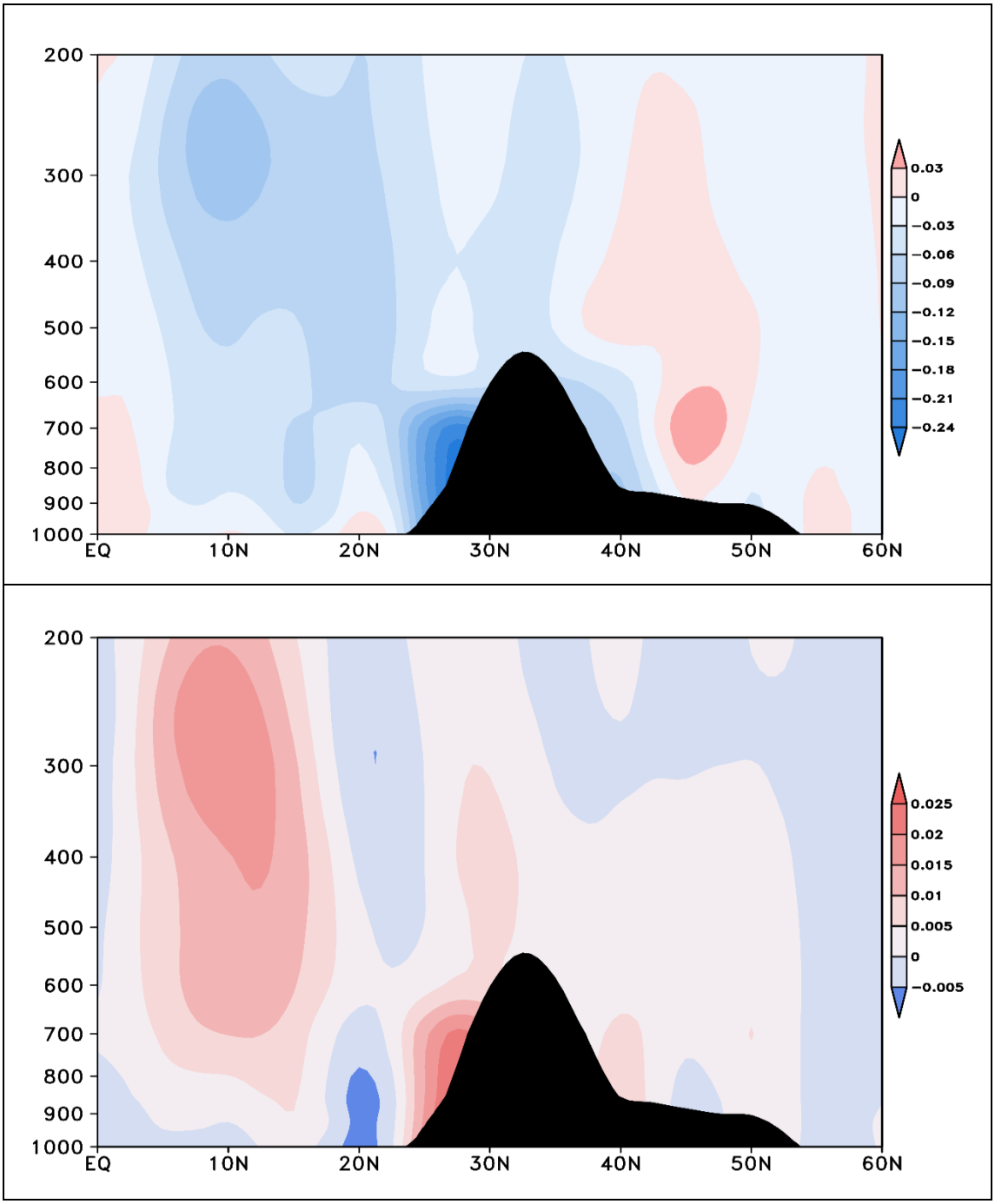

Figure 8. Latitude-vertical sections of vertical velocity climatology (top plot, unit: Pa /s) and trend (bottom plot, unit: Pa/s/decade) over the Tibetan Plateau (85°-90°E) in summer during 1979-2012. Negative/positive values represent uplift/subsidence.

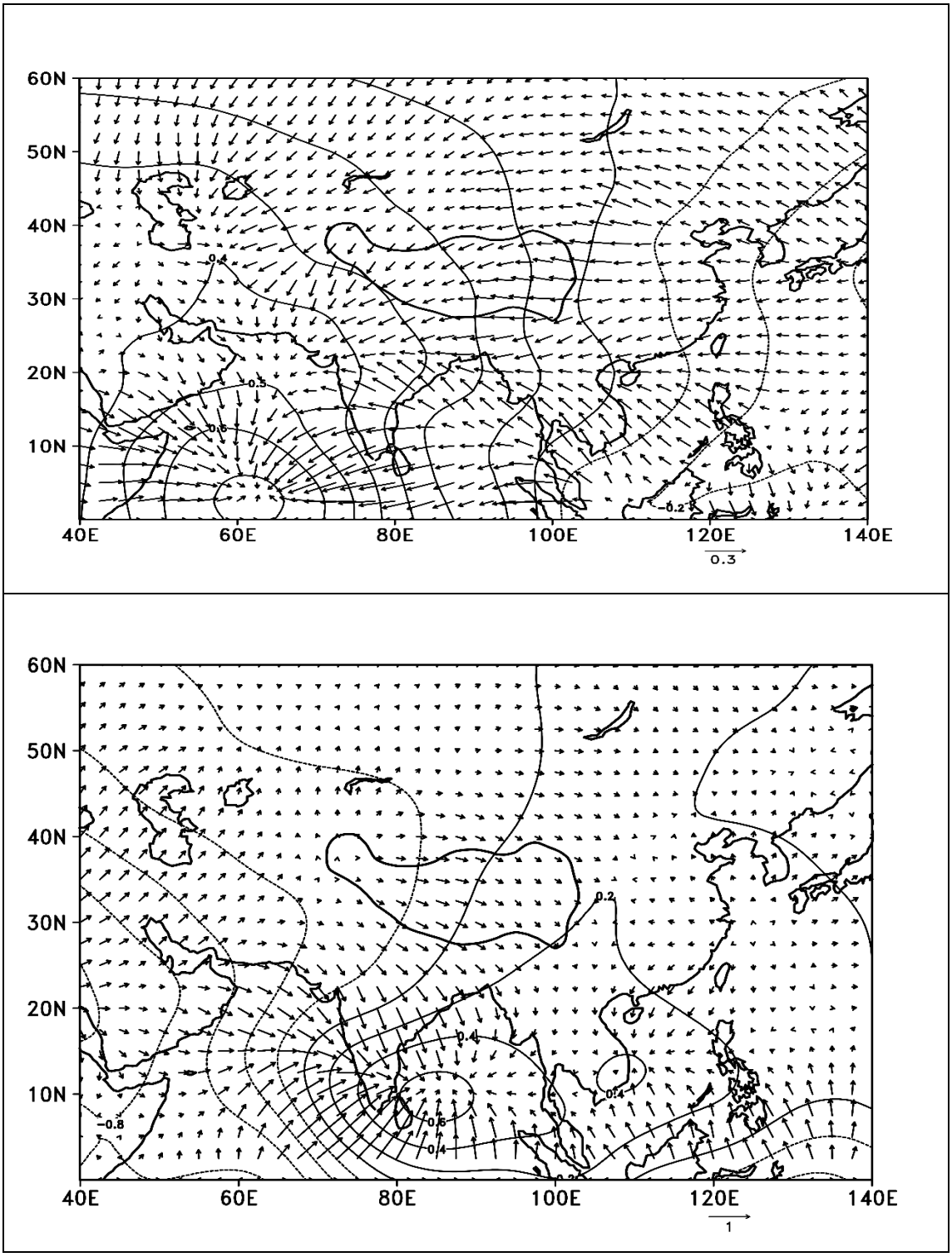

Figure 9. Trends of velocity potential (contour, unit: $10^6 \times m^2/s$/decade,) and divergence (vector, unit m/s/decade) at 400 hPa (top plot) and 200 hPa (bottom plot) in summer during 1979-2012.

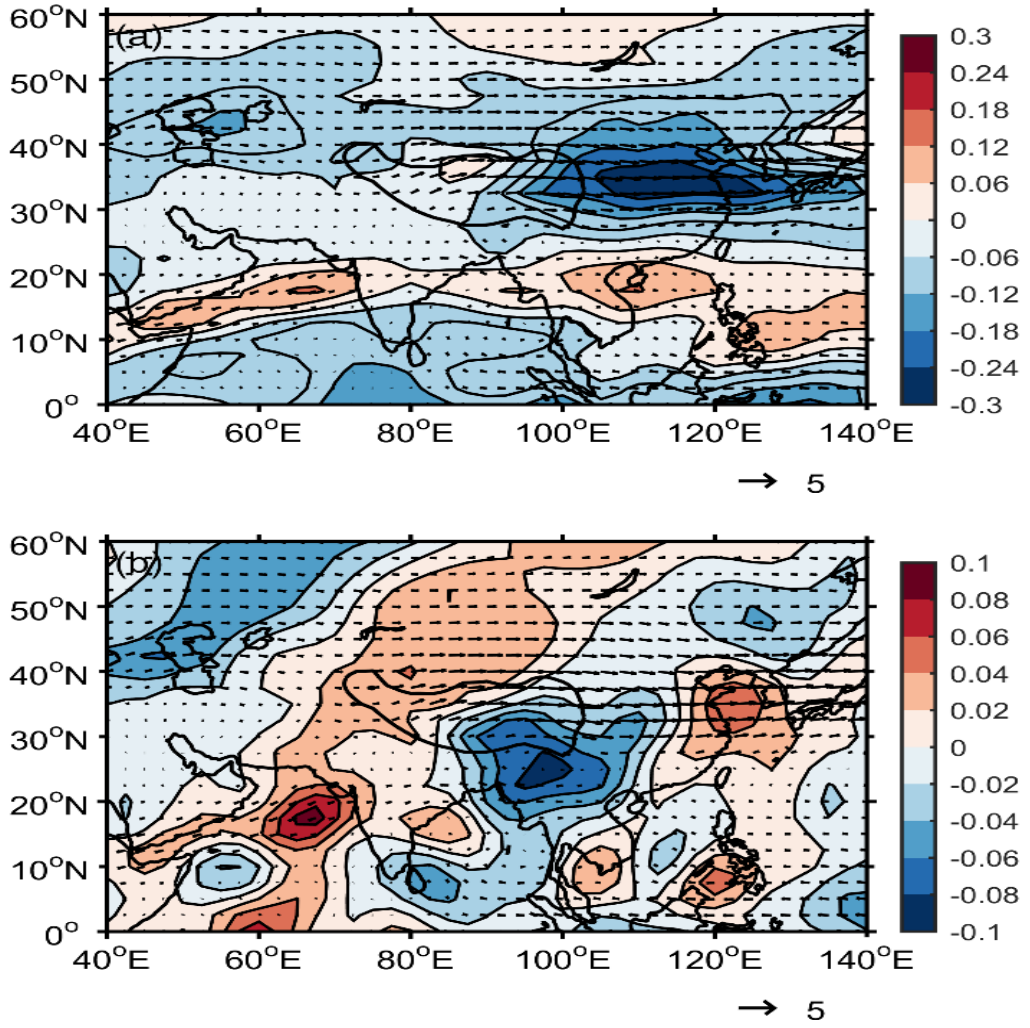

Figure 10. Water vapor flux climatology (vector, unit: g/(s×hPa×cm)) and trend of zonal (top plot) and meridional (bottom plot) water vapor flux (shaded, unit: g/(s×hPa×cm×decade)) at 400hPa in summer during 1979-2012. Positive/negative trends represent wetting/drying respectively.

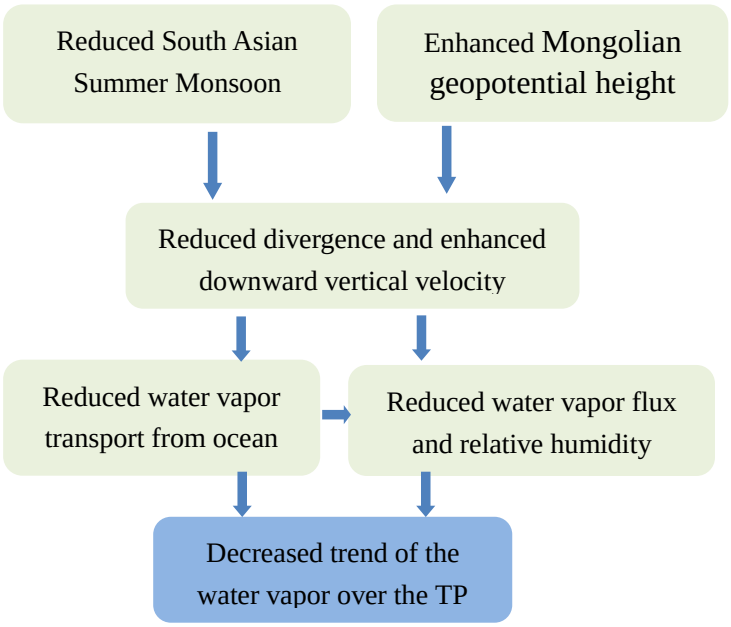

Figure 11. Schematic diagram illustrating the likely factors responsible for the drying trend of HIRS UTWV BT over the Tibetan Plateau.